Supporting Information for

Water Oxidation Catalyzed by Molecular Di- and Nonanuclear Fe complexes: Importance of a Proper Ligand Framework

Biswanath Das,[a] Bao-Lin Lee,[b] Erik A. Karlsson,[b] Torbjörn Åkermark,[b] Andrey Shatskiy,[b] Serhiy Demeshko,[c] Rong-Zhen Liao,[d] Tanja M. Laine,[b] Matti Haukka,[e] Erica Zeglio,[f] Ahmed F. Abdel-Magied,[b] Per E. M. Siegbahn,[b] Franc Meyer,[c] Markus D. Kärkäs,*[b] Eric V. Johnston,*[b] Ebbe Nordlander,[a] and Björn Åkermark*[b]

[a] Inorganic Chemistry Research Group, Chemical Physics, Center for Chemistry and Chemical Engineering, Lund University, Box 124, SE-22100 Lund, Sweden

[b] Department of Organic Chemistry, Arrhenius Laboratory, Stockholm University, SE-106 91 Stockholm, Sweden

[c] Institut für Anorganische Chemie, Georg-August-Universität Göttingen, Tammannstrasse 4, 37077 Göttingen, Germany

[d] Key Laboratory for Large-Format Battery Materials and System, Ministry of Education, School of Chemistry and Chemical Engineering, Huazhong University of Science and Technology Wuhan 430074, China

[e] University of Jyväskylä, Department of Chemistry, PO Box 35, FI-40014 University of Jyväskylä, Finland

[f] Biomolecular and Organic Electronics, Department of Physics Chemistry and Biology, Linköping University, SE-58183 Linköping, Sweden

* E-mail: markus.karkas@su.se, eric.johnston@su.se, bjorn.akermark@su.se

Table of Contents

Materials and general methods

$[Ru(bpy)_3](PF_6)_3$,[S1] $[Ru(bpy)_2(deeb)](PF_6)_2$,[S2] the dinuclear $Fe_2^{III,III}$ complex **5**[S3] and its corresponding ligand[S4] were prepared according to reported procedures. All other reagents including solvents were obtained from commercial suppliers and used directly without further purification. All solvents were dried by standard methods when needed. ^1H and ^{13}C NMR spectra were recorded at 400 MHz and at 100 MHz, respectively. Chemical shifts (δ) are reported in ppm, using the residual solvent peak [$CDCl_3$ (δ(H) = 7.26 and δ(C) = 77.16), [D_6]DMSO (δ(H) = 2.50 and δ(C) = 39.52), [D_4]methanol (δ(H) = 3.31 and δ(C) = 49.00)] as internal standard. Splitting patterns are denoted as s (singlet), d (doublet), t (triplet), q (quartet), m (multiplet), and br (broad). High resolution mass spectra measurements were recorded on a Bruker Daltonics microTOF spectrometer with an electrospray ionizer. IR spectra were recorded on a Perkin-Elmer Spectrum One spectrometer, using samples prepared as KBr discs. The UV-vis absorption spectra were measured on a CARY 300 Bio UV-Visible spectrophotometer. Elemental analyses were carried out at MEDAC Ltd, Chobham, Surrey, United Kingdom. Mössbauer spectra were recorded at 80 K with a ^{57}Co source in a Rh matrix, using an alternating constant-acceleration Wissel Mössbauer spectrometer operated in the transmission mode and equipped with a Janis closed-cycle helium cryostat.

Synthesis

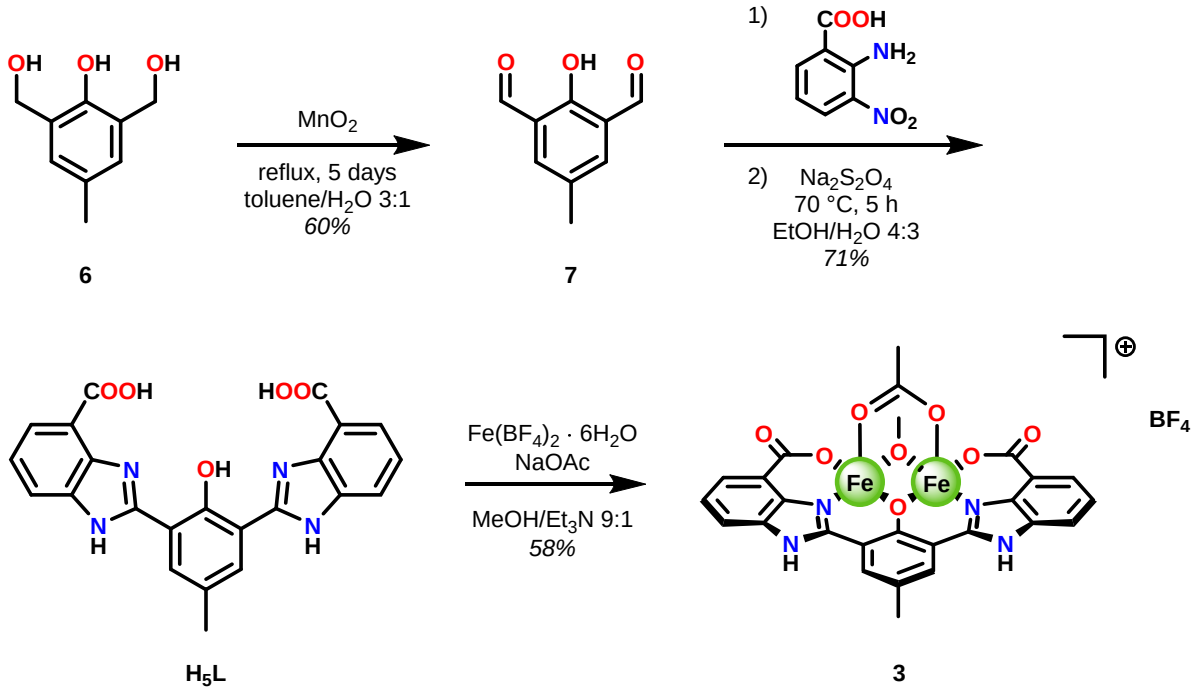

Scheme S1. Synthetic route to ligand H_5L and the dinuclear iron complex **3**.

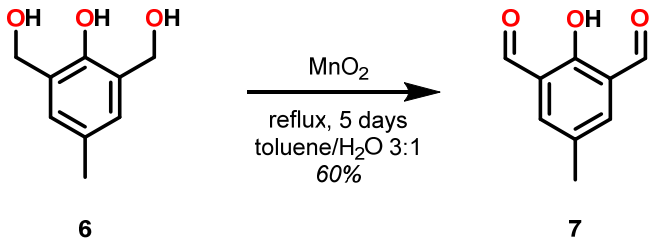

Synthesis of 2-hydroxy-5-methylisophthalaldehyde (7). Activated MnO_2 (103.2 g, 297.3 mmol) was added to a suspension of 2,6-bis(hydroxymethyl)-*p*-cresol (20.00 g, 29.73 mmol) in toluene and H_2O (1.6 L, 3:1 *v/v*). The reaction mixture was refluxed for 5 days and then the reaction mixture was let to reach room temperature, filtered and washed with CH_2Cl_2. The phases were separated and the aqueous phase was washed with CH_2Cl_2. The combined organic phases were dried with Na_2SO_4 and the solvent was evaporated to give the product as a light-yellow solid. (11.62 g, 60%). ^{1}H-NMR (400 MHz, $CDCl_3$) δ: 2.39 (s, 3H), 7.77 (s, 2H), 10.21 (s, 2H), 11.45 (s, 1H); ^{13}C-NMR (100 MHz, $CDCl_3$) δ: 20.2, 123.0, 129.7, 138.1, 161.9, 192.3; HRMS (ESI, MeOH) Calcd. for $C_9H_7O_3$ $[M–H^+]^-$: 163.0401; found: 163.0401.

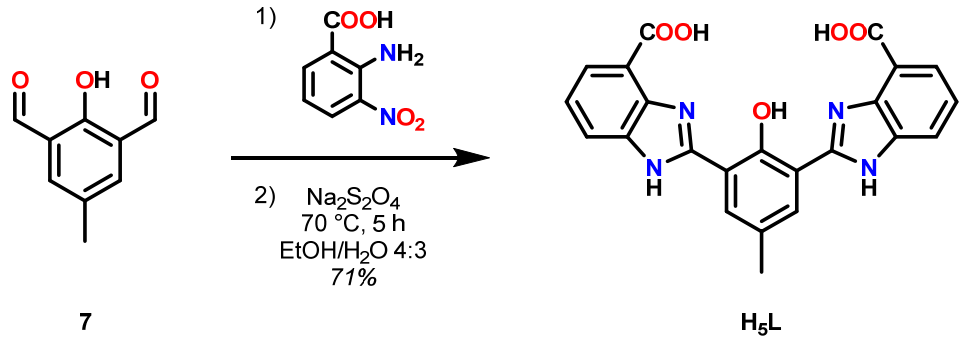

7 **H_5L**

Synthesis of 2,6-bis(4-carboxy-1*H*-benzimidazol-2-yl)-4-methylphenol (H_5L). Using a recently published cyclization procedure,[S5] 2-amino-3-nitrobenzoic acid (3.64 g, 20 mmol) and 2-hydroxy-5-methylisophthalaldehyde (1.64 g, 10 mmol) were dissolved in ethanol (80 ml) at 70 ºC. After cooling to room temperature, a solution of $Na_2S_2O_4$ (85%, 12.29 g, 60 mmol) in water (60 ml) was added. The mixture was then heated at 70 ºC for 5 h. After cooling to room temperature, the red precipitate was filtered off, washed with ethanol, water and acetone, and dried under vacuum affording the title compound as a red solid (3.53 g, 71%). ^{1}H NMR (400 MHz, [D$_6$]DMSO): δ = 8.33 (s, 2 H), 7.95 (dd, J = 7.9, 1.0 Hz, 2 H), 7.84 (dd, J = 7.6, 1.0 Hz, 2 H), 7.35 (dd, J = 7.9, 7.6 Hz, 2 H), 2.41 (s, 3 H). ^{13}C NMR (100 MHz, [D$_6$]DMSO): δ = 167.1, 158.1 (br), 152.6, 141.3, 134.6, 130.9, 125.9 (br), 124.3, 121.8, 121.6 (br), 115.9, 115.0, 20.1; HRMS (ESI, MeOH) Calcd. for $C_{23}H_{15}N_4O_5$ [M–H$^+$]$^-$: 427.1048; found: 427.1033; IR (KBr disc) ν = 3401, 3063, 2923, 1696, 1625, 1565, 1511, 1439, 1380, 1341, 1260, 1209, 1152, 1088, 1046, 990, 873, 787, 755, 741, 637, 619, 604 cm^{-1}; Anal. calcd. for $C_{23}H_{24}N_4O_9$ [**3** · 4H$_2$O]: C 55.20, H 4.83, N 11.20%; found: C 55.44, H 4.61, N 11.04%.

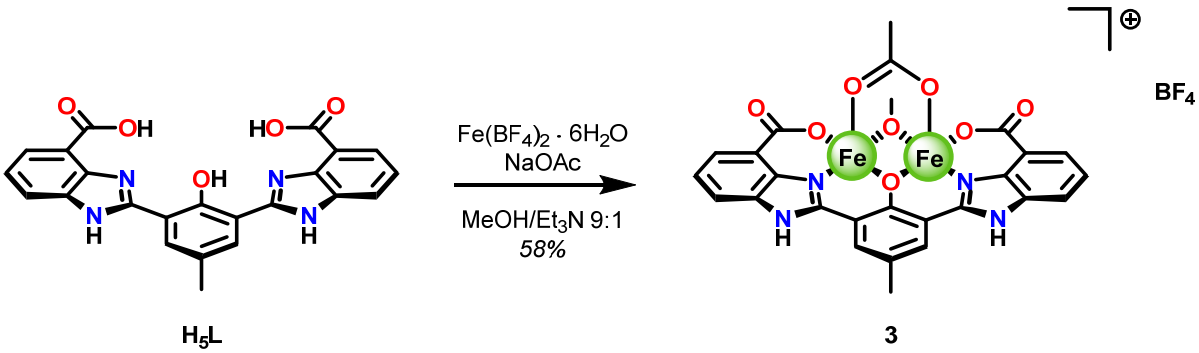

H_5L **3**

Synthesis of $[Fe_2^{III,III}(H_2L)(\mu\text{-}OMe)(OAc)](BF_4)$ ([3](BF_4)). A 5 mL methanolic solution of $Fe(BF_4)_2 \cdot 6H_2O$ (52 mg, 0.154 mmol) was added to a methanol/Et_3N solution (9:1, 10 mL) containing ligand H_5L (33 mg, 0.0771 mmol) and sodium acetate (12.6 mg, 0.154 mmol). This mixture was stirred at room temperature overnight. The solvent was evaporated and the resulting solid was washed with 2 mL cold methanol/Et_3N (9:1) and dried under vacuum to afford the title complex as a dark brown solid (36 mg, 58%). HRMS (ESI, MeOH) Calcd. for $C_{26}H_{17}Fe_2N_4O_8$ $[M–2H^+]^-$: 624.9751; found: 624.9772; IR (KBr disc) ν = 3427.91, 2924.09, 2853.32, 1618.58, 1567.93, 1500.00, 1479.87, 1423.25, 1398.96, 1384.71, 1327.77, 1271.72, 1205.56, 1083.89, 1041.77, 1018.31, 920.38, 898.87, 872.64, 825.88, 775.31, 758.25, 709.73, 645.25, 624.82, 537.12, 512.61, 485.13, 461.31 cm^{-1}; Anal. calcd. for $C_{26}H_{29}BF_4Fe_2N_4O_{13}$ {[**3**]$(BF_4) \cdot 5H_2O$}: C 38.84, H 3.64, N 6.97%; found: C 38.95, H 3.67, N 7.42%.

Synthesis of nonanuclear iron complex 4. A concentrated DMSO solution (2 mL) of the dinuclear Fe complex **3** (50 mg, 0.062 mmol) was heated at 80 °C for 30 min. The resulting turbid black-brown solution was filtered using a 0.45 μm GHP membrane to afford a clear brown filtrate. Upon standing at room temperate over a period of 14 days under aerobic conditions, the clear solution resulted in shining black-brown crystals of the nonanuclear Fe complex **4** (10 mg, 19.3%).

Synthesis of dinuclear iron(III,III) complex 5. Using a previously reported procedure,[S6] NaOAc (0.337 g, 4.11 mmol) was added to a light blue solution of $Fe(ClO_4)_2 \cdot 6H_2O$ (1.02 g, 2.82 mmol) in MeOH (15 mL). Upon addition of the ligand, H_3BBMP (H_3BBMP = 2,6-bis[(2-hydroxybenzyl)(2-pyridylmethyl)-amino-methyl]-4-methylphenol), (0.60 g, 1.07 mmol) the dark brown solution turned deep purple. The reaction mixture was heated at 40 °C for 10 min, upon which a dark blue precipitate

was generated, which was filtered off, washed with isopropanol and ether, and dried over vacuum to give the title complex as a dark blue solid. MS (ESI, MeOH) Calcd. for $C_{40}H_{43}Fe_2N_4O_8$ $[M^+ + MeOH]^+$: 819.18; found: 819.07; IR (KBr disc) ν = 3439.55, 2926.69, 2854.72, 1562.27, 1480.36, 1450.31, 1295.48, 1274.50, 1247.61, 1090.37, 889.61, 791.63, 759.58 cm^{-1}; Anal. calcd. for $C_{43}H_{49}ClFe_2N_4Na_2O_{17}$ {[**5**](ClO_4) · $2H_2O$ · 2NaOAc}: C 47.51, H 4.54, N 5.15%; found: C 47.40, H 4.44, N 5.13%.

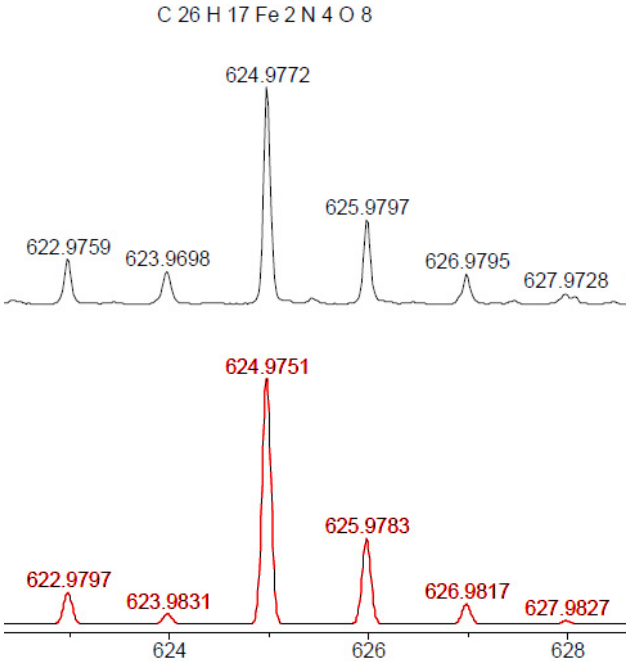

Figure S1. High-resolution ESI-MS spectra of dinuclear iron(III,III) complex **3** ($[\mathbf{3}–2H^+]^–$, $[Fe_2^{III,III}(L)(OAc)(OMe)]^–$) in negative ion mode. Top: experimental spectrum and bottom: calculated spectrum.

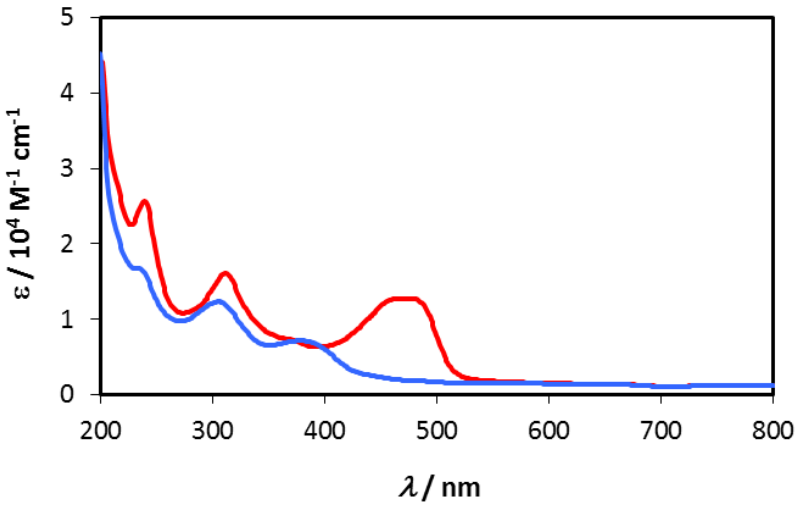

Figure S2. UV-vis absorption spectra of ligand H_5L (—) and iron complex **3** (—) in an aqueous solution at pH 7.2 (0.1 M phosphate buffer).

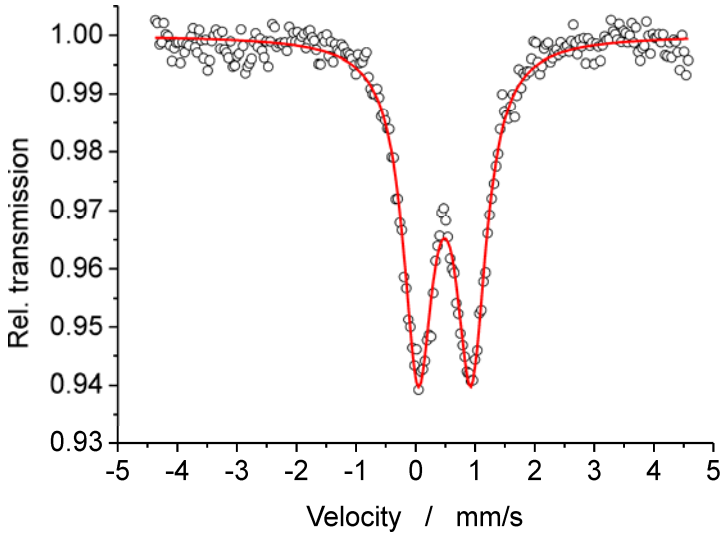

Figure S3. Mössbauer spectrum of iron complex **3**. The red solid line represents a simulation with $\delta = 0.48$ mm s^{-1}, $\Delta E_Q = 0.89$ mm s^{-1} and line width $\Gamma = 0.61$ mm s^{-1}.

Electrochemistry

Electrochemical measurements were carried out in a three-electrode cell with an Autolab potentiostat with a GPES electrochemical interface (Eco Chemie), using a glassy carbon disk (diameter 3 mm) as the working electrode and a platinum coil as counter-electrode. The reference electrode used was a saturated calomel electrode (SCE). The electrolyte used was an aqueous phosphate buffer solution (0.1 M, pH 7.2). All potentials are reported vs. NHE, using the $[Ru(bpy)_3]^{3+}/[Ru(bpy)_3]^{2+}$ couple ($E_{1/2}$ = 1.26 V vs. NHE) as a reference.

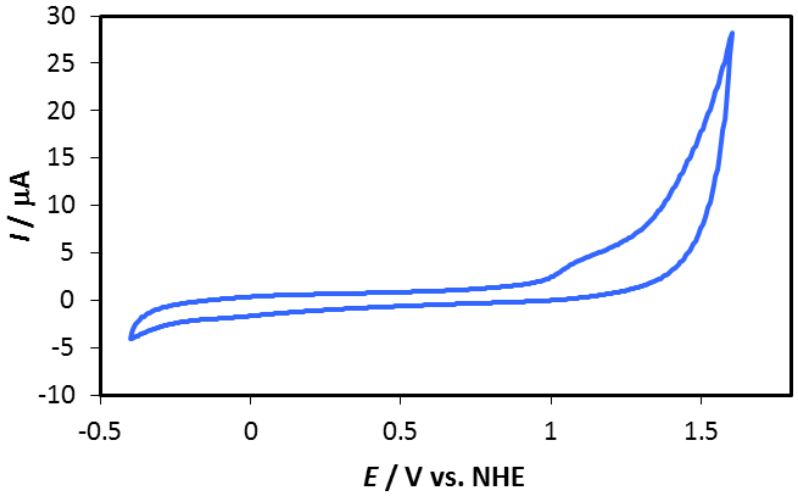

Figure S4. Cyclic voltammogram of dinuclear iron(III,III) complex **3** (0.17 µM) at pH 7.2. Recorded in an aqueous phosphate buffer solution (0.1 M, pH 7.2), at a scan rate of 0.1 V s^{-1} using a glassy carbon disk as the working electrode and a saturated SCE as the reference electrode.

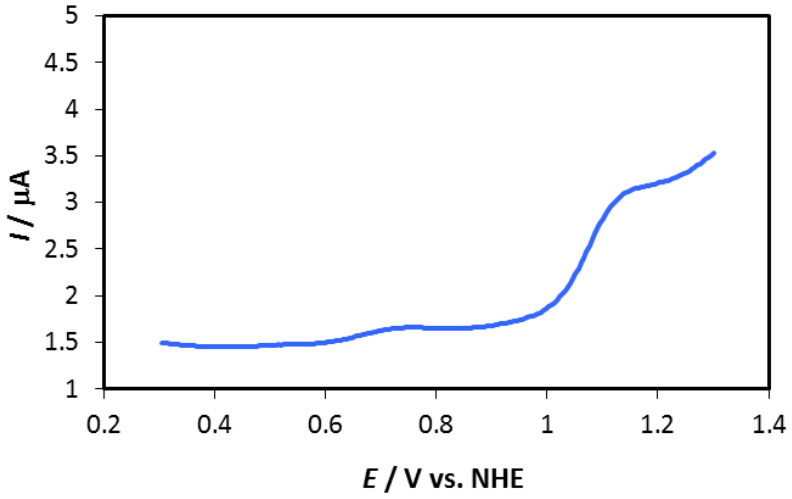

Figure S5. Differential pulse voltammogram of the dinuclear iron(III,III) complex **3** in an aqueous phosphate buffer solution (0.1 M, pH 7.2). Conditions: Recorded at a scan rate of 0.1 V s^{-1} using a glassy carbon disk as the working electrode, a platinum spiral as counter-electrode and a saturated calomel electrode (SCE) as reference electrode.

Oxygen evolution measurements

Oxygen evolution was measured by mass spectrometry (MS).[24,25] An aqueous stock solution was made, containing 1 mM of iron complex and 3.0 mM of K_3PO_4. The catalyst solutions used in the experiments were then made by diluting the stock solutions with phosphate buffer (0.1 M, pH 7.2) to the desired concentrations. The solutions were then deoxygenated by bubbling with N_2 for at least 15 min before being used in the experiments.

Chemical oxidation with $[Ru(bpy)_3](PF_6)_3$

In a typical run, $[Ru(bpy)_3](PF_6)_3$ (3.0 mg, 3.0 µmol) was placed in the reaction chamber and the reaction chamber was evacuated with a rough pump. ~42 mbar He was then introduced into the system. After an additional min the catalyst solution (0.5 mL) was injected into the reaction chamber. The generated oxygen gas was then measured and recorded versus time by MS.

^{18}O-Isotopic experiments

$[Ru(bpy)_3](PF_6)_3$ (3.3 mg, 3.3 μmol) was placed in the reaction chamber and the reaction chamber was evacuated with a rough pump. ~42 mbar He was then introduced into the system and after an additional 5 min $H_2{}^{18}O$ (32 μL) was injected (the ^{18}O concentration in the water was determined from the ratio between *m/z* 18 ($H_2{}^{16}O$) and 20 ($H_2{}^{18}O$)). After an additional 1.5 min the catalyst solution (0.5 mL, 80 μM) was injected into the reaction chamber. The generated oxygen gas was then measured and recorded versus time by mass spectrometry.

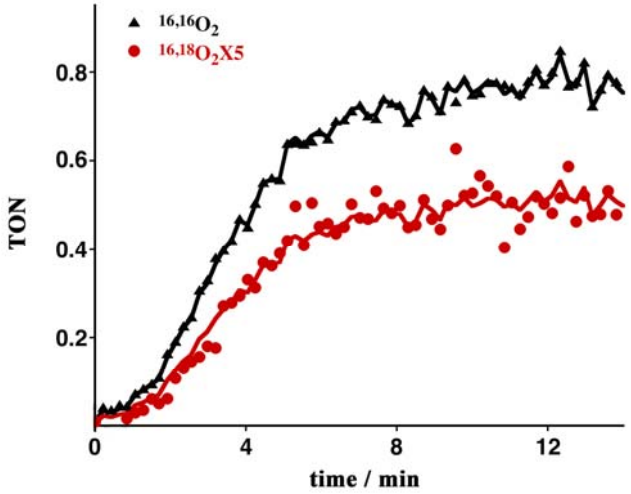

Figure S6. Chemical water oxidation catalyzed by iron complex **3** in isotopically labeled H_2O (6.3% $H_2{}^{18}O$). Experimental conditions: Reactions were carried out in an aqueous phosphate buffer solution (0.095 M, pH 7.2, 0.53 mL, 6.3% $H_2{}^{18}O$) in the presence of complex **3** (80 μM) and $[Ru(bpy)_3](PF_6)_3$ (6.6 mM). $^{16,16}O_2$ measured (▲), $^{16,18}O_2$ measured (●), $^{16,16}O_2$ calculated (—), $^{16,18}O_2$ calculated (—).

Photochemical oxidation with $[Ru(bpy)_2(deeb)](PF_6)_2$ as photosensitizer

In a typical run, $[Ru(bpy)_2(deeb)](PF_6)_2$ in MeCN (0.6 mM) and sodium persulfate (2.5 mg, 10 μmol) were placed in the reaction chamber. The system was then evacuated with a rough pump, removing all MeCN. ~40 mbar He was then introduced into the system. After an additional 5 min, the catalyst solution (80 μM, 0.5 mL) was injected into the reaction chamber and the reaction was irradiated by

visible light. To avoid heating of the reaction by the light source, the reaction vessel was placed in a water bath and cooled with a small flow of water. The generated oxygen gas was measured and recorded versus time by mass spectrometry.

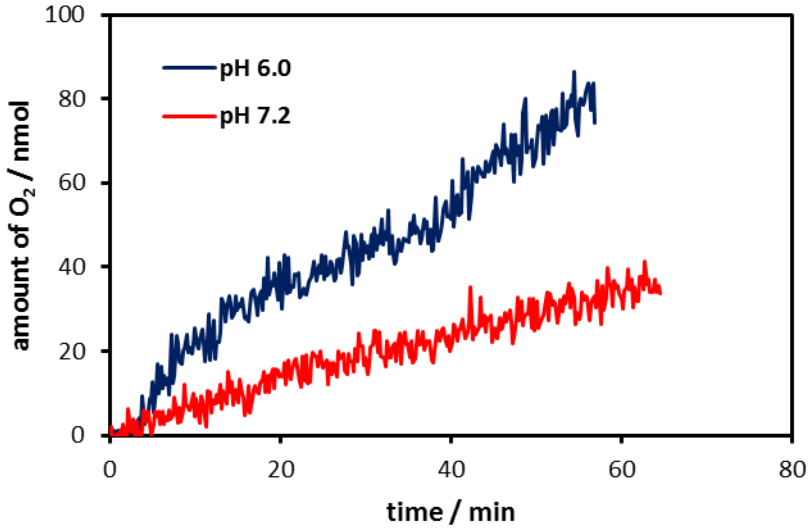

Figure S7. Photochemical water oxidation mediated by dinuclear iron complex **3** at different pH. Experimental conditions: Reactions were performed in an aqueous phosphate buffer solution (0.1 M, pH 7.2, 0.50 mL) containing iron complex **3** (80 μM), $[Ru(bpy)_2(deeb)](PF_6)_2$ as photosensitizer (0.60 mM) and $Na_2S_2O_8$ as sacrificial electron acceptor (20 mM).

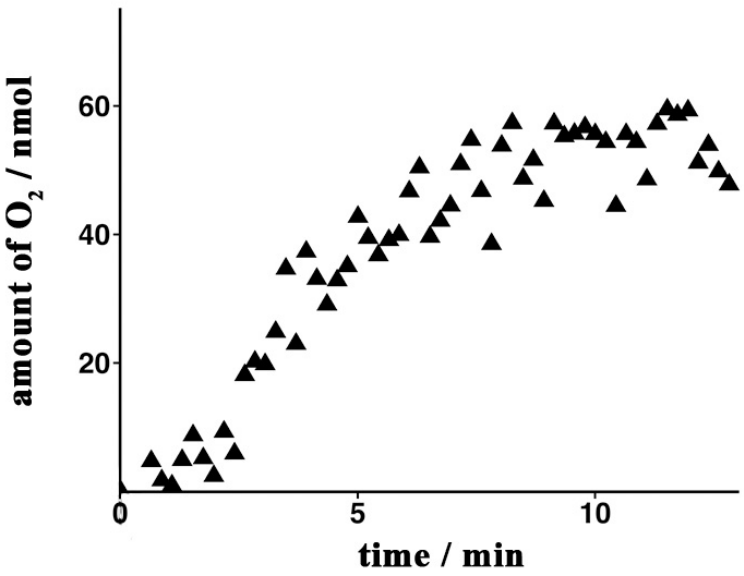

Figure S8. O_2 evolution kinetics by nonanuclear iron complex **4** as a function of time. Conditions: Catalytic water oxidation was performed by adding an aqueous phosphate buffer solution (0.1 M, pH 7.2, 0.50 mL) at 20 ºC containing nonanuclear iron complex **4** (4.4 μM) to the chemical oxidant $[Ru(bpy)_3](PF_6)_3$ (3.0 mg, 3.0 μmol).

Computational details

Geometry optimizations were performed using unrestricted density functional B3LYP[S7] as implemented in the Gaussian09 program.[S8] The standard double-zeta basis set 6-31G(*d,p*) was used for the C, N, O, P, H elements and the SDD[S9] pseudopotential for Fe. The stationary points were characterized by analytic frequency calculations to confirm their character as minima (no imaginary frequencies). On the basis of the optimized structures, more accurate energies were obtained by performing single-point calculations using B3LYP*[S10] with a larger basis set, where all elements, except Fe, were described by 6-311+G(*2df,2p*). The solvation energies from the water solvent were calculated as single-point energy corrections employing the SMD[S11] continuum solvation model with the larger basis set at the B3LYP* level. The reported energies are B3LYP*-D2 energies, including Gibbs free energies corrections from B3LYP and dispersion corrections proposed by Grimme.[S12]

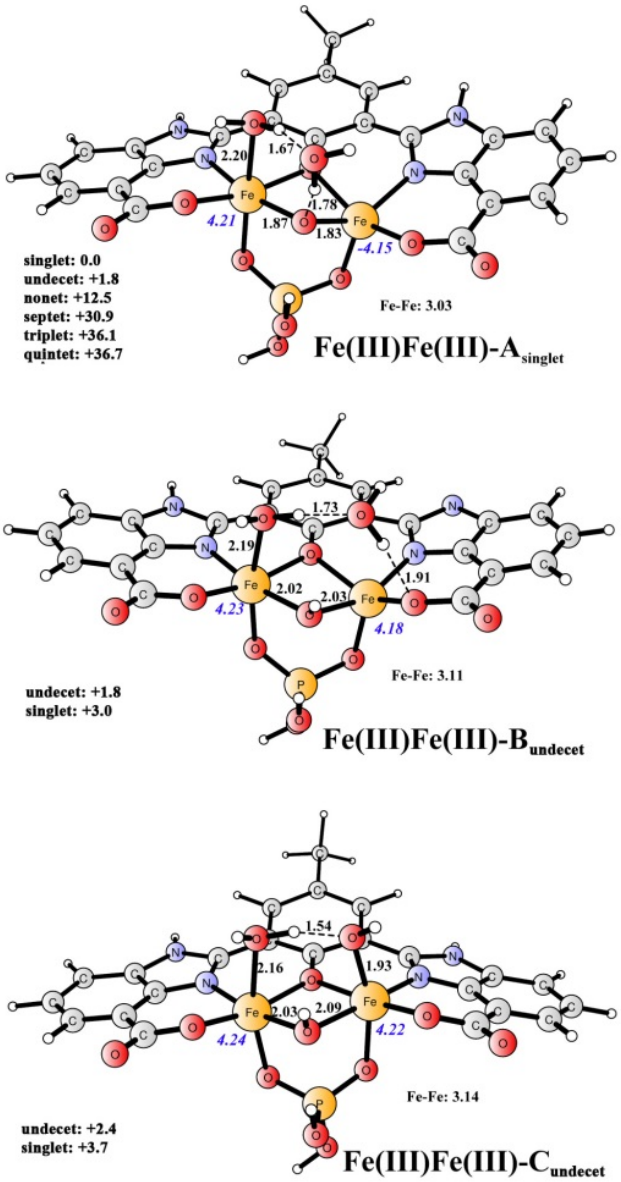

Figure S9. Optimized structures of different isomers of the dinuclear iron(III,III) complex **3** after ligand exchange. Distances are given in Angstrom (A). The relative energies (kcal mol^{-1}) of various spin states are also shown. Spin densities on Fe are shown in *blue italic*.

The calculations revealed that the **Fe(III)Fe(III)-A** isomer had the lowest energy, and both the **Fe(III)Fe(III)-B** and the **Fe(III)Fe(III)-C** isomers lie about 2 kcal mol^{-1} higher in energy. For the **Fe(III)Fe(III)-A** isomer, the antiferromagnetically-coupled singlet is preferred and the ferromagnetically-coupled undecet (S = 5) is 1.8 kcal mol^{-1} higher. A possible explanation could be that the two ferric ions are bridged by an oxo group and the Fe-Fe distance is 3.03 Å, which is about 0.1 Å shorter than the other two isomers. Further calculations on other spin

states, including the nonet, septet, quintet, and triplet states, showed that these states were associated with significantly higher energies (in the range of 12.5–36.7 kcal mol^{-1}), suggesting that both ferric ions prefer to be in the high spin state. For the other two isomers, the high spin undecet ($S = 5$) state was shown to be preferred and the corresponding singlet state was about 1 kcal mol^{-1} higher in energy.

X-ray structure determination

The crystal of **4** was immersed in cryo-oil, mounted in a MiTeGen loop, and measured at a temperature of 123 K. The X-ray diffraction data was collected on a Agilent Supernova diffractometer using Cu Kα radiation (λ = 1.54184 Å). The *CrysAlisPro*[S13] program package was used for cell refinements and data reductions. The structure was solved by charge flipping method using the *Superflip*[S14] program with the *Olex2*[S15] graphical user interface. An empirical absorption correction based on equivalent reflections (*CrysAlisPro*) was applied to the data. Structural refinement was carried out using *SHELXL-2013*.[S16] The crystal under investigation was diffracting only weakly. The crystal structure contained water, acetonitrile and DMSO as solvent of crystallization. One of the acetonitrile molecules was disordered over two sites over with equal occupancies. All solvent molecules could not be unambiguously solved and therefore some of them were omitted from the final structure solution. The contribution of missing solvent to the calculated structure was taken into account using the *SQUEEZE* procedure implemented in *PLATON* software.[S17] Because of the disorder and weak diffraction, a series of constraints and restraints were applied to the structure. Hydrogen atoms were either located from the difference Fourier map and constrained to ride on their parent atom or positioned geometrically and then constrained to ride on their parent atoms, with C–H = 0.95–0.99 Å, N–H = 0.88 Å, and U_{iso} = 1.2–1.5 U_{eq} (parent atom). The crystallographic details are summarized in Table S1.

CCDC 966406 contains the supplementary crystallographic data for this paper. The data can be obtained free of charge from The Cambridge Crystallographic Data Centre via www.ccdc.cam.ac.uk/data_request/cif.

Table S1. Crystal data and structure refinement for the nonanuclear iron cluster **4**.

Identification code	**4**
Empirical formula	$C_{452}H_{363}Fe_{27}N_{73}O_{147}S_{18}$
Formula weight	11254.16
T (K)	123(2)
λ (Å)	1.54184
Crystal system	Trigonal
Space group	P-31c
a (Å)	27.7653(7)
b (Å)	27.7653(7)
c (Å)	44.8044(17)
α (deg)	90
β (deg)	90
γ (deg)	120
V (Å^3)	29912.8(19)
Z	2
ρ_{calc} (Mg/m^3)	1.249
μ (Mo Kα) (mm^{-1})	6.309
No. reflns.	58624
Unique reflns.	17980
GOOF (F^2)	0.972
R_{int}	0.0802
$R1$[a] ($I \geq 2\sigma$)	0.0955
w$R2$[b] ($I \geq 2\sigma$)	0.2672

[a] $R1 = \Sigma||F_o| - |F_c||/\Sigma|F_o|$. [b] $wR2 = [\Sigma[w(F_o^2 - F_c^2)^2]/ \Sigma[w(F_o^2)^2]]^{1/2}$.

Dynamic light scattering (DLS)

Dynamic light scattering experiments were performed using uniphase He-Ne laser emitting light at a wavelength of 632 nm (power 22 mW) and two avalanche photo diodes (PerkinElmer, Canada) working in cross auto correlation mode. Data was collected at 294 ± 0.5 K. The scattering angle was set to 90° from the incident laser. The intensity correlation curves were analyzed with an ALV-500/E/EPP + ALV-60XO-win V3.0.2.3 software. CONTIN deconvolution algorithm was used to obtain the intensity distribution of the relaxation times. The corresponding radius values were calculated using the Stokes-Einstein equation. Number weighted particle radius distribution functions were obtained by weighting the amplitudes of the intensity distribution..

In a series of dynamic light scattering (DLS) experiments at pH 7.2 (0.1 M phosphate buffer), no trace of nanoparticle formation (1–1000 nm) was detected within 10 min after mixing iron complex **3** (50 µM) and $[Ru(bpy)_3](PF_6)_3$ (5 mM) (Figure S10a) and in a separate experiment iron cluster **4** (5 µM) and $[Ru(bpy)_3](PF_6)_3$ (1.0 mM) (Figure S10b). All the stock solutions were filtered using a 0.45 µm filter before mixing and no further filtration were performed afterwards.

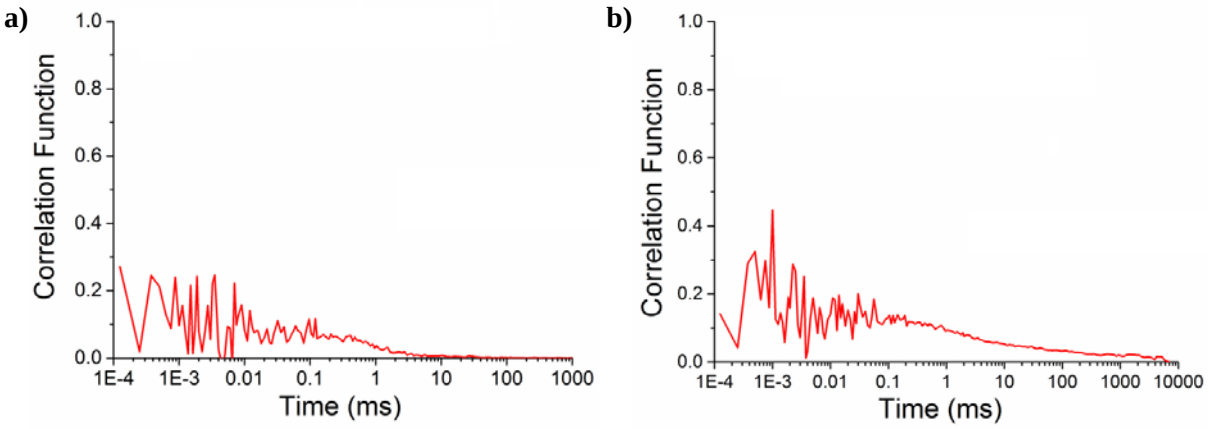

Figure S10. Correlation function versus time (ms) plot of the dynamic light scattering experiments using (a) complex **3** and (b) complex **4**.

Using a similar technique and set up but in a different experiment, nanoparticle formation (hydrodynamic radius ~90 nm) was observed when $Co(NO_3)_2$ was used. Correlation diagram and

number distribution diagrams for the solution ($Co(NO_3)_2$ and $[Ru(bpy)_3](PF_6)_3$ at pH 8.0 (borate buffer, 0.1 M) are depicted in Figure S11a and Figure S11b, respectively.

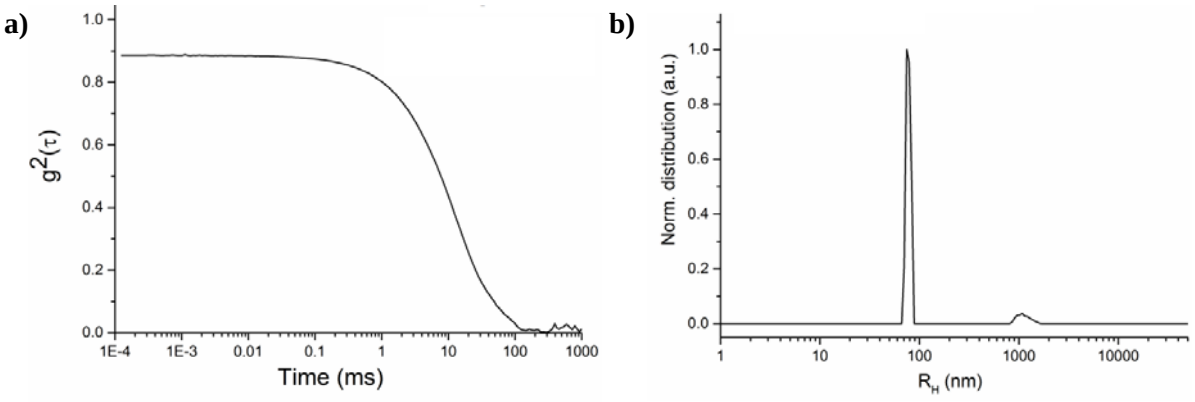

Figure S11. Correlation diagram (a) and number distribution diagram (b) of the dynamic light scattering experiment using $Co(NO_3)_2$.

Supporting references

(S1) R. E. DeSimone and R. S. Drago, *J. Am. Chem. Soc*., 1970, **92**, 2343–2352.

(S2) (a) B. P. Sullivan, D. J. Salmon and T. J. Meyer, *Inorg. Chem*., 1978, **17**, 3334–3341; (b) A. R. Oki and R. J. Morgan, *Synthetic Communications*, 1995, **25**, 4093–4097; (c) H. Xia, Y. Zhu, D. Lu, M. Li, C. Zhang, B. Yang and Y. Ma, *J. Phys. Chem. B*., 2006, **110**, 18718–18723.

(S3) A. Neves, M. A. de Brito, I. Vencato, V. Drago, K. Griesar and W. Haase, *Inorg. Chem*., 1996, **35**, 2360–2368.

(S4) B.-L. Lee, M. D. Kärkäs, E. V. Johnston, A. K. Inge, L.-H. Tran, Y. Xu, Ö. Hansson, X. Zou and B. Åkermark, *Eur. J. Inorg. Chem*., 2010, 5462–5470.

(S5) D. Yang, D. Fokas, J. Li, L. Yu and C. M. Baldino, *Synthesis*, 2005, 47–56.

(S6) A. Neves, M. A. de Brito, I. Vencato, V. Drago, K. Griesar and W. Haase, *Inorg. Chem*., 1996, **35**, 2360–2368.

(S7) A. D. Becke, *J. Chem. Phys*., 1993, **98**, 5648–5652.

(S8) M. J. Frisch, G. W. Trucks, H. B. Schlegel, G. E. Scuseria, M. A. Robb, J. R. Cheeseman, G. Scalmani, V. Barone, B. Mennucci, G. A. Petersson, *et. al*. Gaussian 09, Revision B.01, Gaussian, Inc. Wallingford CT, **2009**.

(S9) D. Andrae, U. Häußermann, M. Dolg, H. Stoll and H. Preuß, *Theor. Chim. Acta*., 1990, **77**, 123–141.

(S10) M. Reiher, O. Salomon and B. A. Hess, *Theor. Chem. Acc*., 2001, **107**, 48–55.

(S11) A. V. Marenich, C. J. Cramer and D. G. Truhlar, *J. Phys. Chem. B*, 2009, **113**, 6378–6396.

(S12) S. Grimme, *J. Comput. Chem*., 2006, **27**, 1787–1799.

(S13) L. Palatinus and G. Chapuis, *J. Appl. Cryst*., 2007, **40**, 786–790.

(S14) Agilent, *CrysAlisPro*, Agilent Technologies Inc. **2013**, Yarnton, Oxfordshire, England.

(S15) O. V. Dolomanov, L. J. Bourhis, R. J. Gildea, J. A. K. Howard and H. Puschmann, *J. Appl. Cryst*., 2009, **42**, 339–341.

(S16) G. M. Sheldrick, *Acta Cryst*., 2008, **A64**, 112–122.

(S17) A. L. Spek, *Acta Cryst*., 2009, **D65**, 148–155.